IEEE Access
Multidisciplinary | Rapid Review | Open Access Journal

Received 7 June 2022, accepted 22 July 2022, date of publication 1 August 2022, date of current version 4 August 2022.

Digital Object Identifier 10.1109/ACCESS.2022.3195273

RESEARCH ARTICLE

Radar Signals Intrapulse Modulation Recognition Using Phase-Based STFT and BiLSTM

SIDRA GHAYOUR BHATTI, (Member, IEEE), AND AAMER IQBAL BHATTI, (Senior Member, IEEE)
Department of Electrical Engineering, Capital University of Science and Technology, Islamabad 45750, Pakistan
Corresponding author: Sidra Ghayour Bhatti (dee193001@cust.pk)

ABSTRACT The goal of radar emitter recognition (RER) is to extract the features of the received emitter signal. This has become a critical issue as new radar types are emerging, and the electromagnetic environment is becoming denser and more complex. Deep neural networks (DNNs) have recently proven effective for emitter identification; however, the recognition of phase-coded waveforms at a low signal to noise ratio (SNR) remains challenging. In this paper, a novel phase-based RER approach using short time fourier transform (STFT) and bidirectional long short term memory (BiLSTM) is proposed, while enhancing the ability to learn features from noisy signals. The phase spectrum of phase-coded signals was analyzed in contrast to the amplitude spectrum used in state-of-the-art approaches in the literature. The derived phase-based features were directly provided as inputs to the proposed BiLSTM architecture. The fully connected layer follows the BiLSTM layer. Finally, a softmax classifier was employed to accomplish the recognition task. Six distinct types of phase-coded waveforms degraded by additive white gaussian noise (AWGN) with SNRs ranging from −8 dB to 8 dB were simulated. The method proposed in this research involves simple pre-processing and exhibits an overall recognition accuracy of more than 90% at SNR of −2 dB.

INDEX TERMS Bidirectional long short term memory (BiLSTM), emitter identification, phase coded waveforms, time-frequency transform, deep neural network.

I. INTRODUCTION

The complexity of today's radar environment makes it difficult to distinguish between the different threat signals present in a measured spectrum. The rapid advancement of radar design theory and manufacturing technology leads to a growing number of new radar types [1], [2]. These characteristics make the recognition of radar signals extremely difficult [3]. It is very hard to create a radar emitter recognition (RER) system that can perform efficiently with a variety of radar types. Low probability of intercept (LPI) radars are specially designed radars that try to obscure their emissions from hostile receivers including radar warning receivers (RWRs) [4]–[6]. A typical way to realize LPI radar signals is to reduce the radar's peak effective radiated power (ERP) using pulse compression techniques. The use of intrapulse modulation for pulse compression is very effective. It has a high bandwidth-time product and large radar signal processing gain [7]. The transmitted pulse is either frequency or phase-modulated to increase the bandwidth. The top-level diagram for an airborne RWR is shown in Fig. 1. The process of emitter recognition, which is an important technology in the field of electronic countermeasures, is as follows: first, the radar signal is preprocessed; then, the preprocessed signal is analyzed to identify the intrapulse modulation schemes used by threat emitters. The extraction of these characteristics investigates the model of threat emitter, function, threat level, and other information to distinguish enemy radars. RER technology has evolved through different stages. In the first stage, traditional methods using the parameter matching approach were used to match the intrapulse parameters of intercepted signals with the information maintained in a database [8]–[10]. Radar signal identification has made a lot of progress after decades of research.

The associate editor coordinating the review of this manuscript and approving it for publication was Nikhil Padhi.

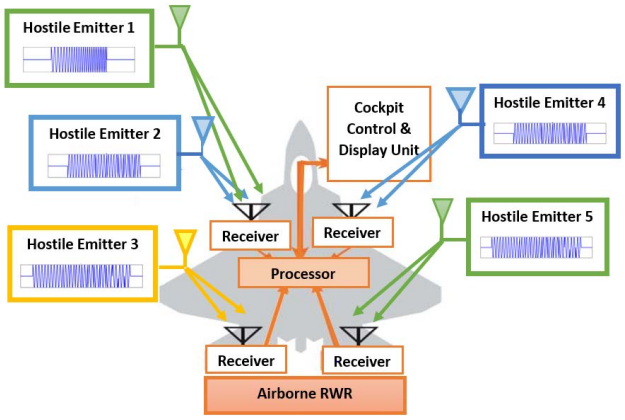

FIGURE 1. Signals received at RWR by multiple threat emitters.

Deep learning has made significant progress in this field. In the second step, artificial intelligence technology is used to integrate the intelligence component into the parameter matching approach. Deep learning methods, which are based primarily on the time-frequency transform fall under the third category. LPI radar signals are non-stationary so the time-frequency transforms are widely used for feature extraction [11], such as smoothed pseudo wigner ville distribution (SPWVD) [12], wigner ville distribution (WVD) [13], short-time fourier transform (STFT) [14], [15], choi-william distribution (CWD) [16], stockwell transform (ST) [17], and fourier based synchro squeezed transform (FSST) [18].

A. RELATED WORK IN MACHINE LEARNING

Deep learning has attracted much interest in the field of automatic radar waveform recognition and has increased the recognition accuracy of radar emitter signals [19]. In [20], a recognition approach based on convolutional neural networks (CNN) and sample averaging techniques (SAT) is proposed, however FRANK, P1, and P4 signals still need to enhance their recognition rates. Furthermore, the problem of identifying Barker codes has yet to be overcome. Lunden in [21] proposes a supervised classification technique based on features extracted from received pulses. The overall recognition rate is 98% at signal to noise ratio (SNR) of 6 dB. A novel technique based on intrapulse parameters is proposed in [22] using the variant of STFT and reinforced deep belief network (RDBN) but linear frequency modulation (LFM) and non-linear frequency modulation (NLFM) get confused with other modulation schemes. The modulation classification problem is considered in [23] when the intercepted radar signals are sent using radio over fiber networks. It is observed that at SNR of -2 dB the recognition accuracies of phase coded signals is less. A novel 1D deep residual shrinkage network (DRSN) based radar emitter recognition method is provided in [24]. The recognition accuracies of phase-coded signals are not considered in this research. A waveform categorization method based on the FSST combined with deep learning is used in [25]. However, for low SNR levels, the proposed approach has less capability to differentiate between LFM and Costas codes.

B. RELATED WORK IN REFERENCE TO LSTM

In RER algorithms, recurrent neural networks (RNNs) are used to categorize the intercepted signals and is used for de-noising, classification, and de-interleaving of pulse streams [26]. The phase-based radar sequences are not used at the input of RNN. In [12], a hybrid network built on a shallow CNN, LSTM, and DNN is proposed that can recognize six distinct radar emitter signals with SNRs ranging from -14 dB to 20 dB. The suggested approach, however, does not address the identification of polyphase-coded waveforms. In [27], a novel recognition approach based on CNN-LSTM and STFT is presented. The suggested method can identify eight distinct radar signals with an overall accuracy of 96% at an SNR of -2 dB. However, the recognition accuracies of polyphase coded signals other than P2 are not discussed. The multiple feature images joint decision (MFIJD) model with two different feature extraction structures is proposed in [28]. It is observed that Structure 2 is based upon LSTM and has less recognition accuracy for phase-coded signals at low SNR values. For decades, identifying the different Intrapulse modulation techniques used by LPI radar waveforms has been a major research challenge.

In most state-of-the-art techniques, low recognition accuracies are observed for phase-coded signals using the magnitude spectrum at low SNR values [29]. In this work, we propose a phase spectrum-based feature extraction method as phase should be an important candidate for the recognition of phase-coded signals. We are filling the gap to achieve good recognition accuracies at low SNR by investigating the phase spectrum of the phase-coded waveforms.

C. PAPER's CONTRIBUTION

To the best of our knowledge and comparison of some previous works the main contribution of this paper is summarized in the subsequent points:

1) A novel feature vector based on phase information is derived from noisy emitter signals and is given at the input of bidirectional long short term memory (BiLSTM) network.
2) A DNN model based on BiLSTM architecture is proposed where mini-batch processing allows for anti-causal behavior and effectively increases the amount of data accessible to the network at every time step, providing the algorithm richer context.
3) The identification accuracies of phase-coded signals including Barker codes at low SNR levels are compared with other state-of-the-art techniques in the literature.

The remainder of this paper is structured as follows. LPI radar waveforms, including Barker and polyphase codes, are discussed in Section II along with the feature extraction using STFT. The system overview is given in section III. The proposed phase-based emitter recognition algorithm

using the BiLSTM network is explained in section IV. Section V contains the simulations and performance evaluations. In Section VI, the suggested method is compared to existing state-of-the-art techniques in the literature. The conclusion of the whole work is drawn in section VII.

II. THEORETICAL BACKGROUND

In this section, LPI radar waveforms are discussed along with the proposed phase-based feature extraction method using STFT.

A. PHASE CODED LPI RADAR WAVEFORMS

In the LPI radar system, a long-duration pulse is phase or frequency modulated before transmission, and the received signal is then passed through a matched filter to concentrate the energy into a shorter pulse. Barker, Frank, P1, P2, P3, and P4 codes are among the phase-coded signals utilized in our research.

1) BARKER CODE

The Barker codes are a collection of binary phases with a peak-to-peak side lobe ratio of M (Length of code). Barker codes are not defined for M>13, and the sidelobe level ratio for the largest length code is observed to be −22.3 dB. Binary phase modulation is commonly used in Barker-coded pulses and they offer low complexity [30]. These codes have the unity magnitude side lobes and are only available for lengths, M= 2, 3, 4, 5, 7, 11, and 13.

Polyphase modulation refers to the exploitation of several phase values to modulate long-duration pulses. Lower sidelobes are produced using polyphase codes as compared to biphase codes. This subsection introduces the mathematical definition of polyphase-coded waveforms.

2) FRANK CODE

Frank proposed a polyphase code with good non-periodic correlation properties named as Frank code. The Frank code is a perfect code derived from the phase history of the LFM pulse. Only perfect square length ($N = L^2$) is applicable with this code. The formula for generating phases of sub-pulses is expressed in (1).

$$\phi_{m,n} = \frac{2\pi}{L}(m-1)(n-1) \tag{1}$$

where, $1 \leq m \leq L$ and $1 \leq n \leq L$. In Frank code, the middle of the code has the largest phase increments as compared to both ends [30].

3) P1 CODE

Both P1 and P2 codes are obtained from the step approximation of an LFM signal. The length of the code is ($N = L^2$) [30]. If m denotes a sample number in a given n^{th} frequency step, then the phase value of the m^{th} sample of the n^{th} frequency step can be calculated by using (2).

$$\phi_{m,n} = -\frac{\pi}{L}[L-(2n-1)][(n-1)L+(m-1)] \tag{2}$$

where, m= 1, 2, 3, ….., L, n= 1, 2, 3,….., L and N should be a perfect square length. Peak sidelobe level (PSL) for P1 code is expressed by using the formula:

$$PSL = 20log_{10}\left(\frac{1}{L\pi}\right) \tag{3}$$

4) P2 CODE

The P2 code works for perfect square lengths as well, although even values of L result in low-level autocorrelation sidelobes. P2 has the same phase increments as P1, but the initial phase values are different [30]. The following formula is used to calculate the phase values for sub-pulses:

$$\phi_{m,n} = -\frac{\pi}{2L}[2m-1-L][2n-1-L] \tag{4}$$

where, m= 1, 2, 3,…, L, n= 1, 2, 3, …, L and L= 2, 4, 6, …High phase increments are observed at both ends of the code relative to the middle of the code for both P1 and P2 codes.

5) P3 CODE

P3 and P4 codes are derived from the approximation of Zadoff-Chu given in [31], which are valid for any length N_c. The formula given in (11) may be used to compute the phase of the mth sample of the P3 code [30].

$$\phi_m = -\frac{\pi}{N_c}(m-1)^2 \tag{5}$$

where, $m = 1, 2, \ldots, N_c$, and N_c is the compression ratio.

6) P4 CODE

The phase values of a P4 code are described by the formula given in [30]:

$$\phi_m = -\left[\frac{\pi(m-1)^2}{N_c}\right] - \pi(m-1) \tag{6}$$

where, m= 1, 2, …., N_c. The P3 code varies from the P4 code in that it has the largest phase increments in the middle, similar to the Frank code. P3 and P4 codes, in comparison to other polyphase codes, are more Doppler resistant.

B. NOVEL PHASE-BASED FEATURE EXTRACTION

Feature extraction helps in the reduction of unnecessary data that accelerates the learning and generalization stages of the machine learning algorithm. In this work, the phase-based feature is extracted using STFT. It is most extensively used, simple to interpret, and has speedy implementations [32]–[34].

$$X(m,\omega) = \sum_{n=-\infty}^{\infty} x[n]\omega[n-m]e^{-j\omega n} \tag{7}$$

where, $x[n]$ is the signal and $w[n]$ is the window used for computing STFT. In the literature [24]–[27], feature extraction is usually done using amplitude values obtained from time-frequency transforms. We have computed phase values from the output of the STFTs. Phase offset is intentionally introduced in the phase-coded waveform at the transmission side.

This waveform is eventually intercepted by the electronic warfare (EW) receiver. It is intended to measure the phase offsets introduced by the emitter in the intercepted waveform during the phase coding process. These measured offsets will help in recognizing the unknown phase coding scheme used by the emitter.

1) OPTIMAL WINDOW SIZE FOR FEATURE EXTRACTION

It is imperative that the window of data samples used for phase offset estimation should be short enough to ensure that the phase offset of each sub-pulse remains intact. The optimal window size is chosen to get more precise phase information and the carrier must complete its one cycle within that window. The duration of the sub-pulse is usually longer than that of a carrier cycle so the phase offset remains unchanged within the measured window. For STFT calculations, the window length (samples) and the number of fast fourier transform (FFT) points are kept uniform.

2) STEPS FOR PHASE-BASED FEATURE EXTRACTION

The detailed algorithm for phase-based feature extraction is outlined in the flowchart shown in Fig. 2 and is divided into two parts; Detection Problem and Recognition Problem. In Detection Problem, the carrier frequency of intercepted noisy signal is determined using following steps:

1) The modulated discrete signal corrupted with additive white gaussian noise (AWGN) is intercepted at the EW receiver and its FFT is computed.
2) The absolute value of the FFT result is obtained and the frequency corresponding to the maximum value is identified known as carrier frequency F_c.
3) The reciprocal of F_c is computed to obtain the time required by the carrier to complete its one cycle known as T_c.

$$T_c = \frac{1}{F_c} \tag{8}$$

4) T_c is multiplied with a sampling frequency F_s to obtain the window size in terms of samples. T_s is the sampling time.

$$window(samples) = T_c * F_s \tag{9}$$

$$window(time) = T_s * window(samples) \tag{10}$$

After determining the F_c and optimal window size, the Recognition Problem is encountered that consists of following steps:

1) The window is slid over the signal for the first time to obtain a column vector with a length equal to FFT points.
2) The maximum value is determined from the column obtained and its phase is computed that corresponds to the phase offset of the carrier frequency signal.
3) The window is ultimately slid over the entire length of a signal and the STFT is computed window-wise.
4) The phase value acquired from each window is recorded in a pre-initialized vector and ultimately a phase-based feature vector for each corresponding signal is obtained.
5) The feature vector is further provided as an input to the BiLSTM network for recognition.
6) The above process is repeated for all the intercepted signals at different SNR values.
7) The efficacy of the trained BiLSTM network is evaluated by using the testing dataset containing signals of different SNRs ranging from −8 dB to 8 dB.

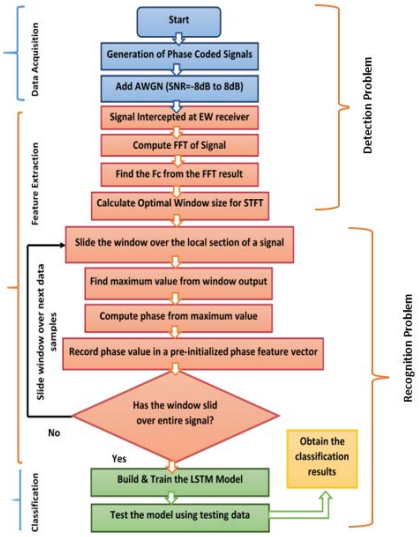

FIGURE 2. Flowchart of phase-based feature extraction algorithm.

The phase features derived using the proposed method are shown in Fig. 3 for specific phase-coded signals at different SNR values. The phase of actual Barker Code (Length=13) without AWGN is shown in Fig. 3a, which serves as a benchmark. The Barker Code (Length=4) is the shortest length signal used for simulations that can be obtained within $2\mu s$. It is practically viable to do recognition on the basis of overall phase feature vector of this signal. Time duration of signals are shown on the x-axis, while phase values (degree) are shown on the y-axis. The phase is 0° from 0μs till 5μs and 180° for 5μs through 7μs. From 7μs to 9μs, it switches to 0°, and so on. The extracted phase feature vectors of Barker Code are displayed in Fig. 3b, Fig. 3c, and Fig. 3d for SNR values of 2 dB, 0 dB, and −2 dB, respectively. Although the phase fluctuations of retrieved Barker code features are nearly identical to those of benchmark code but they are noisy since AWGN is present. Similarly, the phases of other signals are compared to their respective benchmark codes and are shown in Fig.3d till Fig.3x. The tangent inverse is used to compute the phase of the STFT output. Since the tangent's period is π, whenever the phase value exceeds 180° on both the positive and negative sides due to noise, wrapping occurs, which is obvious in plots.

3) PHASE-BASED FEATURE IMAGES USING STFT

The phase-based feature images produced for the Barker code of length (M=13) and the Frank code of length (L=6, N=36)

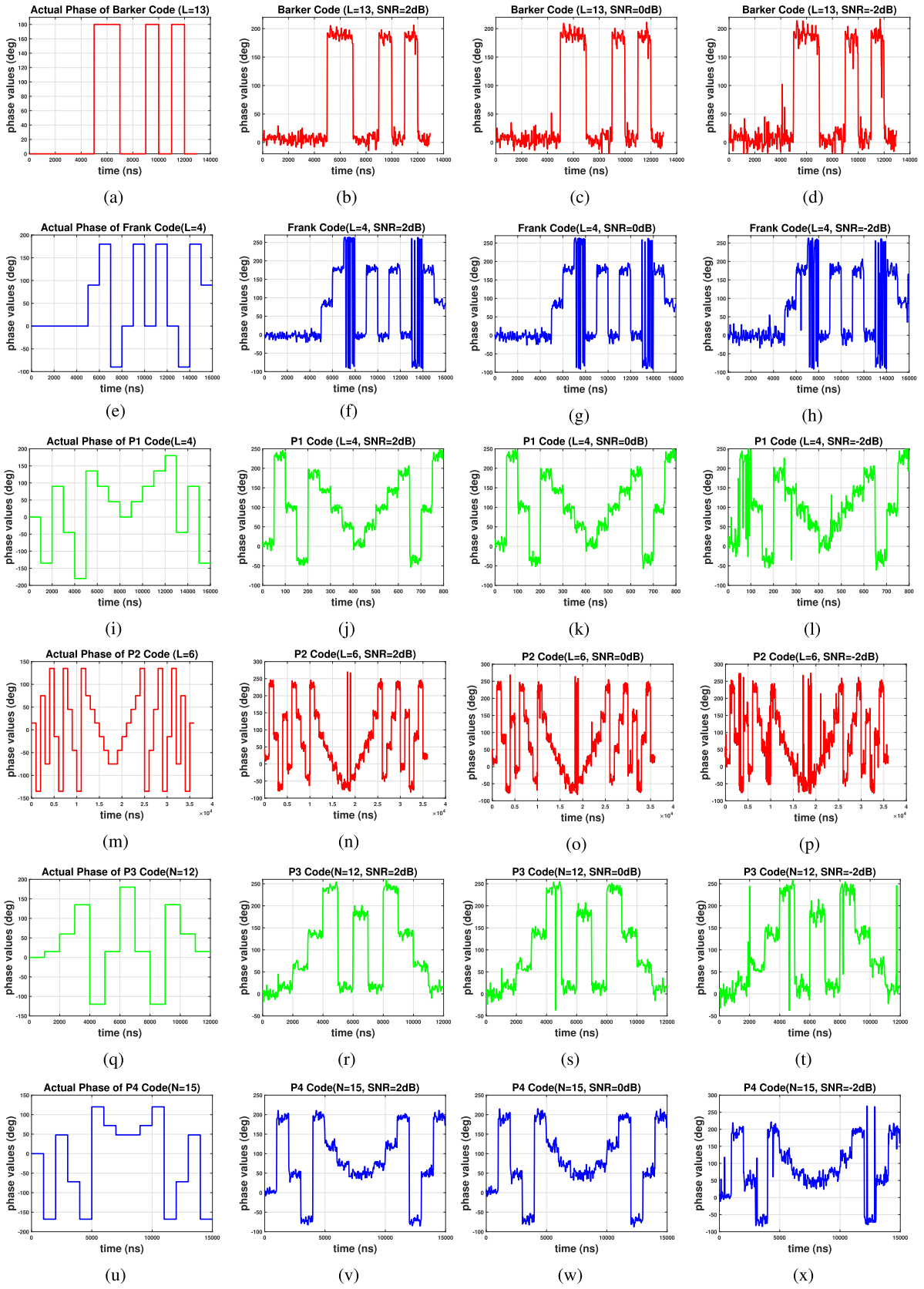

FIGURE 3. Examples of phase features derived from phase-coded signals at different SNR ratios using the proposed technique.

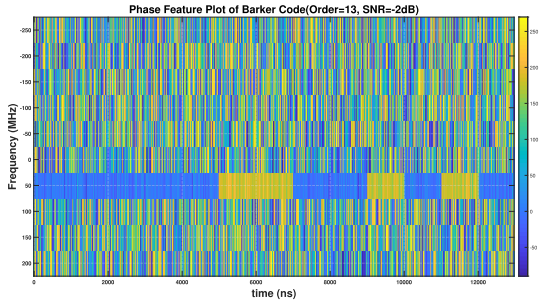

FIGURE 4. Phase Feature Plot of Barker Code (Length=13, SNR=−2 dB).

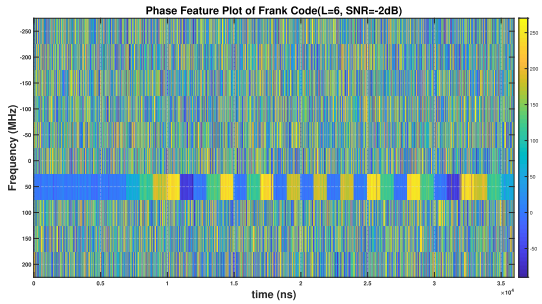

FIGURE 5. Phase Feature Plot of Frank Code (L=6, SNR=−2 dB).

are presented in Fig. 4 and Fig. 5, respectively. Both plots are given for SNR= −2dB. If we follow the detailed steps of the detection part in the algorithm then Fc and window size can be calculated. The window is moved over entire length of signal, and the phase values from each window output are horizontally stacked, producing a 2D matrix. The heatmap (image) of the 2D matrix is then generated. These images have nothing to do with the simulations; they are only intended to illustrate how phase values appear on a frequency versus time graph (STFT). The seventh row in the plots in both Fig. 4 and Fig. 5 corresponds to the phase offset of carrier signal introduced by the particular modulation schemes and is given as a feature vector to the BiLSTM network. The remaining rows correspond to the noise.

III. SYSTEM OVERVIEW

This section involves a detailed overview of the overall recognition system. The proposed identification system, as shown in Fig. 6, is composed of three main components: time-frequency transform, phase-based feature extraction, and a classification network. In the first step, STFT is computed for all waveforms. Using the appropriate window size for STFT, the phase of output is computed. The second step involves the formation of a phase-based feature vector that will be further provided at the input of the BiLSTM network in third step for recognition purposes. The system collects a lot of information about various types of waveforms after the first and second parts, then all waveforms are classified in the third section. The classifier can distinguish between six different types of phase coded waveforms including Barker, Frank, P1, P2, P3, and P4.

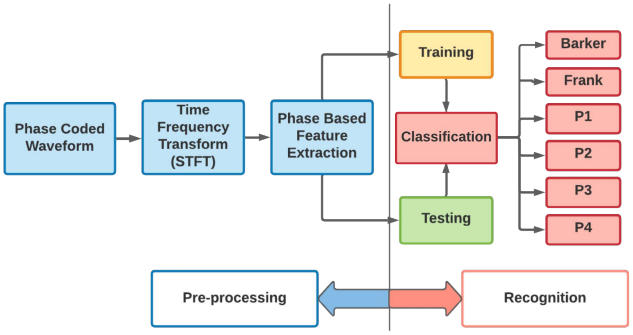

FIGURE 6. Proposed recognition method is divided into three main steps. In the first step, STFT is applied to all phase-coded signals. The second step involves the computation of a phase-based feature vector that is further provided at the input of the BiLSTM network in the third step.

IV. PHASE BASED EMITTER RECOGNITION USING BILSTM NETWORK

In this section, the proposed emitter recognition method is explained in detail along with the function of the BiLSTM network.

For the past few decades, deep learning algorithms have been well researched and frequently used to extract information from various kinds of data. Artificial neural network (ANN), Elman network, CNN, deep belief network (DBN), and RNN are some of the deep learning architectures used for LPI radar waveform recognition applications, as mentioned in [24]–[26]. DNN and CNN are mostly incapable of retrieving temporal information from given data. RNNs are commonly utilized in applications that include sequential data such as audio, text, and video. RNNs are incapable to deal with cases when there is a wide gap between the current input and relevant information. Hochreiter [35] suggested an LSTM network that can handle long-term dependence in the given time series. Several isomorphic cells exist in LSTM that can store information for a long period by updating the internal state.

A. BILSTM NETWORK DESIGN

The Forget gate, Cell state (memory), Input gate, and Output gate are the four main elements of each BiLSTM cell. Emitter recognition using the BiLSTM architecture is shown in Fig. 7. The functions of these gates is explained below:

1) FORGET GATE

The initial task of LSTM is to figure out which data is valuable and which should be discarded. The "Forget Gate," which contains the sigmoid layer is responsible for this decision. It looks at the current input x_t and previous recurrent information h_{t-1} and returns a value that could be 1 or 0.

$$f_t = \sigma(W_f.[h_{t-1}, x_t] + b_f) \tag{11}$$

Here, b_f is the bias term for forget gate and W_f are the weights; σ represents the sigmoid activation function.

2) INPUT GATE

The input gate regulates how the current cell state is updated in response to the current input. It is divided into two main

sections. The "Input Gate," a sigmoid layer, determines which values need to be modified first. Second, a tanh layer creates a new vector called $\tilde{C}_t$, which is then added to the cell state as expressed in (13).

$$i_t = \sigma(W_i.[h_{t-1}, x_t] + b_i) \tag{12}$$

$$\tilde{C}_t = \tanh(W_c.[h_{t-1}, x_t] + b_c) \tag{13}$$

where b_i is the bias term for input gate and W_i are the corresponding weights; b_c and W_c are the bias term and weights for updating cell state.

3) CELL STATE

The current cell state C_t is obtained by updating the past cell state C_{t-1}. The old cell state is multiplied by the output of forget gate and then an update to cell state $\tilde{C}_t$ is multiplied by the input gate. Both candidates are then added to update the cell state.

$$C_t = (f_t * C_{t-1} + i_t * \tilde{C}_t) \tag{14}$$

4) OUTPUT GATE

Finally, a decision has to be made about what should be sent to the output. This will require the cell state to be updated. The sigmoid is used in the first stage to determine what should be given at the output. The state of the cell is then passed through the tanh layer and multiplied by the output of the Output gate.

$$o_t = \sigma(W_o.[h_{t-1}, x_t] + b_o) \tag{15}$$

$$h_t = o_t * tanh(C_t) \tag{16}$$

where b_o is the bias term for output gate and W_o are the weights; h_t represents the current recurrent information. The gate structure has been deliberately designed to address the problem of vanishing or exploding gradients in RNN. The BiLSTM is a network model that consists of two LSTMs, one of which accepts input in one direction while the other takes input in the opposite direction. The BiLSTM reverses the input sequence and calculates the output in the same way as an LSTM layer. The end result is a stack of forward and reverse LSTMs that achieve the goal of incorporating contextual information. As compared to LSTM networks, BiLSTM networks learn faster. Forward propagation is used twice in such networks to train both forward and backward cells. The final output is denoted by y_t, which may be stated as follows:

$$y_t = [h_t{}^f, \ h_t{}^b] \tag{17}$$

Here, t= 1,2,3, …, n, represents the time steps. Hence, both the forward $h_t{}^f$ and backward activations $h_t{}^b$ are used to calculate the output at any time instant t.

V. SIMULATION RESULTS

In this section, we simulate different kinds of phase coded signals to test the efficacy of the proposed recognition algorithm. MATLAB 2021b is used to simulate all of the generated data and results. Each waveform has its own set of parameters that should be adjusted.

A. SIMULATION SETTINGS

The performance of the suggested classification method is tested by utilizing six different types of phase-modulated signals, including Barker, Frank, P1, P2, P3, and P4 codes. The sampling frequency is F_s =500 MHz and the carrier wave frequency is F_c =50 MHz for all signals. For simulation purposes, intermediate frequency (IF) signals are assumed. The pulse width varies, but the pulse repetition interval (PRI) for all signals is considered to be 0.2 ms. The Barker code elements of length (M= 4, 7, 11, and 13) are used in the simulation having the pulse widths of 2 μs, 14 μs, 11 μs and 13 μs respectively. The Frank codes are generated for (L= 3, 4, and 6) using the formula mentioned in section II having the pulse widths of 9 μs, 16 μs, and 36 μs respectively. Similarly, P1 codes are produced for lengths (L= 2, 4) having the pulse widths 8 μs, and 16 μs respectively. Using the formula given in section II, the P2 codes are generated for lengths (L= 4, and 6) having the pulse widths of 16 μs, and 36 μs respectively. P3 codes are developed for lengths (N_c= 4, 12, 16) with the pulse widths of 8 μs, 12 μs, and 16 μs respectively. Signals are created for lengths (N_c= 4, 12, 15) with pulse widths of 8 μs, 12 μs, and 15 μs, respectively, using P4 codes. The parameters of simulated phase-coded signals are given in Table 1. The model's output is the category labels of the emitters. At each SNR value, number of samples for Barker, Frank, P1, P2, P3, and P4 codes are 20000, 35000, 12000, 16000, 28000, and 17500 respectively. There are total 17 signals belonging to six different categories of phase coded waveforms as mentioned earlier. At each SNR value, AWGN is added to signals five times for generating training dataset. There are nine SNR values ranging from −8 dB to 8 dB with a stepzize of 2dB.

$$\text{Training signals (total)} = 17X5X9 = 765 \text{ signals} \tag{18}$$

$$\text{Testing signals (at each SNR)} = 17X5 = 85 \text{ signals} \tag{19}$$

After the various emitter signals are simulated with different phase coding schemes, the proposed BiLSTM network is trained using 765 signals for six different types of phase-coded waveforms. We divide the labels into two parts, 80% labels for training and 20% for validation. The ability of BiLSTM network to recognize phase-coded signals is tested using the testing dataset containing 85 signals at each SNR value ranging from −8 dB to 8 dB and their confusion matrices are also given in this section.

B. NETWORK PARAMETERS

For our classifier model to perform classification tasks, hidden nodes in the BiLSTM layer, network depth, activation functions, and other parameters are all established. The input and recurrent weights are initialized randomly using a Gaussian distribution with a 0 mean and a standard deviation of 0.01. For all gates, the initial bias terms are set to zero. Training epochs are also important throughout the learning phase. In our BiLSTM design, the network is trained with

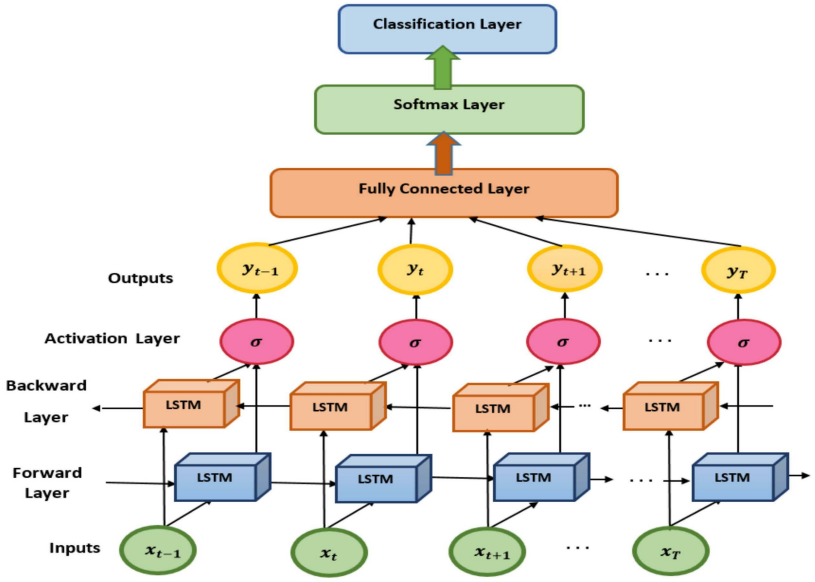

FIGURE 7. BiLSTM Architecture for recognition of phase coded signals.

TABLE 1. Parameters Settings of Radar Signals.

Modulation Type	Parameters	Values
Barker	Carrier Frequency (F_c) Order of Code (L)	50 MHz [3,4,7,11]
Frank	Carrier Frequency (F_c) Cycles per phase code (cpp) Frequency Steps (L)	50 MHz [100,50,50] [3,4,6]
P1	Carrier Frequency (F_c) Cycles per phase code (cpp) Frequency Steps (L)	50 MHz [100,50] [2,4]
P2	Carrier Frequency (F_c) Cycles per phase code (cpp) Frequency Steps (L)	50 MHz [50,50] [4,6]
P3	Carrier Frequency (F_c) Cycles per phase code (cpp) Compression ratio (N_c)	50 MHz [100,50,50] [4,12,16]
P4	Carrier Frequency (F_c) Cycles per phase code (cpp) Compression ratio (N_c)	50 MHz [100,50,50] [4,12,15]

TABLE 2. Training Parameters for BiLSTM Architecture.

Parameters	Values
No of BiLSTM Layers	1
Hidden Units (BiLSTM Layer)	110
Activation Function	tanh, sigmoid
Epochs	100
Optimizer	Adam
Mini-Batch Size	383
Sequence Length	According to longest sequence
Learning Rate	0.01
Learning rate (drop rate)	0.1
Shuffle	Once every epoch
Gradient Threshold	1

only 100 epochs and hidden nodes for the BiLSTM network are kept as 110. The Adam optimizer is used to acquire the best-learned weights. The mini-batch size is kept 383 signals for each training iteration which is half of total training signals. The initial learning rate for training is 0.01. The learning rate schedule is piecewise, the software changes it every 50 epochs by multiplying it by 0.1. The validation frequency is kept as 20 so that the network will be validated after 20 iterations during the training process. The gradient threshold is taken 1 and the length of sequence for a single iteration of the mini-batch is adjusted by the network itself. The best training parameters chosen for simulation are given in Table 2 along with their values.

C. RECOGNITION RESULTS

The number of misrecognition is calculated by comparing the recognition results to the testing labels. The confusion matrix is used to analyze the effectiveness of the algorithm as well as to estimate the recognition accuracies of the phase-coded waveform for testing datasets. Radar emitter identification accuracy (RERA) is plotted versus SNR ranging from -8 dB to 8 dB as shown in Fig. 8. Each waveform has its unique relationship between SNR and RERA. All waveforms in our system have a positive correlation between SNR and RERA. When SNR is less than -2 dB, RERA increases significantly for all phase-coded waveforms. The majority of waveforms have a RERA of 90% at -2 dB, except P1 codes. The overall accuracy for all codes is about 90% at an SNR of -2 dB.

The confusion matrix is shown in Fig. 9 that represents the testing accuracies of phase-coded waveforms at the SNR of -4dB. The recognition accuracies of codes are given in the bottom row of the confusion matrix. Barker, P2, and P4 codes have about 90% recognition accuracies as compared to other codes. Frank code has an accuracy of 86.7%, P1 has 50%, whereas P3 has 80% as it is confused with Barker code. The overall recognition accuracies of all phase-coded

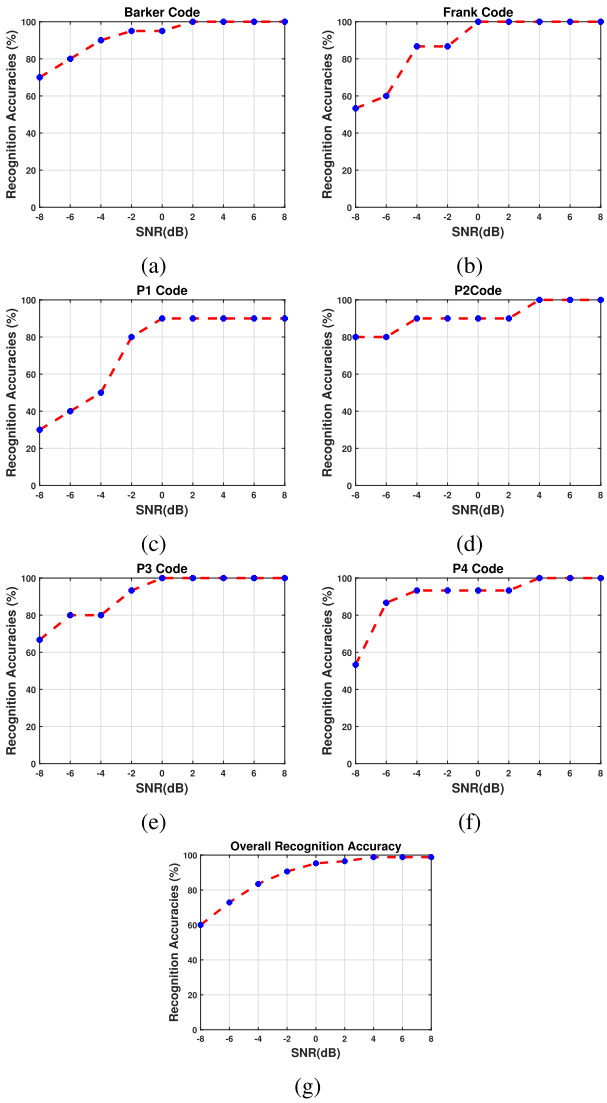

FIGURE 8. Recognition accuracies of phase coded waveforms versus SNR (a) Barker, (b) Frank, (c) P1, (d) P2, (e) P3, (f) P4 (g) Overall Recognition accuracies for all phase coded waveforms.

waveforms using the proposed algorithm are observed to be 83.5% at SNR of −4dB. Similarly, as shown in Fig. 10, the confusion matrix is displayed at SNR of −2dB. More than 90% accuracy is observed for Barker, P3, and P4 codes. P2 code has an accuracy of 90%, 86.7% for Frank, and 80% for P1 code as it gets confused with P4 code.

VI. DISCUSSION AND COMPARISON

In this subsection, the suggested RER methodology is compared to other state-of-the-art methods reported in the literature. In terms of the SNR requirement, the suggested approach is compared to the other methods given in [19], [23], and [28].

1) COMPARISON WITH [23]

In [23], the recognition accuracies of polyphase coded signals are given under the effect of Gaussian noise at SNR=−2 dB.

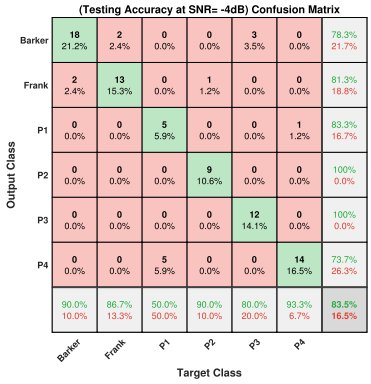

FIGURE 9. Confusion Matrix for the testing dataset at SNR of −4 dB.

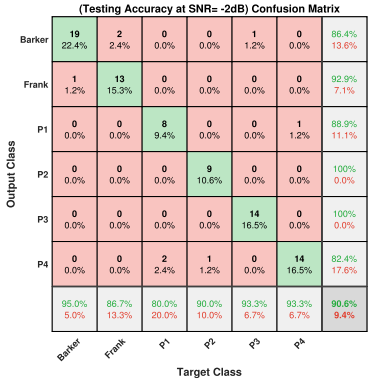

FIGURE 10. Confusion Matrix for the testing dataset at SNR of −2 dB.

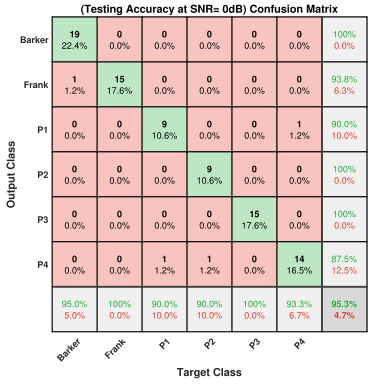

FIGURE 11. Confusion Matrix for the testing dataset at SNR of 0 dB.

It is observed that recognition rates for P2, P3, and P4 codes have improved using our proposed method. The recognition rate has reduced for P1 code as it got confused with the P4 code. The Frank code needs further improvement in their recognition accuracy. Moreover, Barker codes have 95% recognition accuracy.

2) COMPARISON WITH [19]

A hybrid classifier model based on CNN and elman neural network (ENN) method for identifying twelve different types of radar waveforms is proposed in [19]. Recognition

TABLE 3. Comparison of Radar Emitter Recognition Accuracy (RERA) with [23] and [19] at SNR of −2 dB.

Phase Coding Types	[23] (-2 dB)	[19] (-2 dB)	Proposed Method (-2 dB)
Barker	Not given	Not given	95
Frank	100	90	86.7
P1	95	87.5	80
P2	87	90	90
P3	76	78.5	93.3
P4	92	69	93.3

TABLE 4. Comparison of Radar Emitter Recognition Accuracy (RERA) with [28] at SNR of 0 dB.

Phase Coding Types	[28] (0 dB)	Proposed Method (0 dB)
Barker	Not given	95
Frank	99.5	100
P1	87	90
P2	100	90
P3	100	100
P4	88	93.3

accuracies for P3 and P4 codes have improved by using our proposed method, but recognition rates for P1 and Frank codes have reduced as they got confused with other codes at low SNR values. The P2 code exhibits uniform recognition accuracy in both methods. Furthermore, the performance of Barker code is also explored in this paper.

3) COMPARISON WITH [28]

In [28], two structures are adapted to determine the recognition accuracies of polyphase coded signals and the comparison is done with structure 2 that contains combined CNN and LSTM architecture. It has been noticed that adopting our proposed method, recognition rates for Frank, P1, and P4 codes have improved, however, recognition rates for P2 codes have decreased in our work. In both techniques, the P3 code has a 100% recognition accuracy. Moreover, the performance of Barker codes is not discussed in this work.

The results achieved in this research are comparable to the above mentioned state-of-the-art methods. Our suggested approach does not require any complex pre-processing and is best suited for online recognition of phase-coded signals at the EW receiver side. However, the proposed work contains certain inconsistencies that need to be addressed. Frank codes are confused with Barker codes at low SNR levels. Similarly, the phase patterns of P1 and P4 codes are very similar, thus they are mixed up at low SNR resulting in lower recognition accuracies.

VII. CONCLUSION

This paper proposes a novel emitter recognition approach based on the STFT and BiLSTM network to enhance the recognition accuracies of phase-coded waveforms at low SNR values. The proposed technique operates well in practice, with 90% overall identification accuracies for six different types of emitter waveforms at the SNR of −2 dB. The experimental results show that employing the BiLSTM framework using phase-based feature extraction, recognition accuracies of polyphase coded signals have improved when compared to other approaches in the literature. The proposed research does not involve any complex pre-processing, and the feature extraction is performed on the noisy and modulated phase-coded signals obtained at EW receivers. This technique can be beneficial while performing online recognition of phase-coded waveforms as less processing time is required. Furthermore, Barker codes have a good recognition accuracy even at low SNR, but they are rarely discussed in the literature. In the future, researchers can explore more advanced deep learning methods to determine an unknown number of radar signals in a more realistic environment as well as the combined version of different phase-coded signals.

ACKNOWLEDGMENT

The authors sincerely appreciate the reviewers for their constructive feedback and recommendations, which helped to make the paper even better. Special thanks to Abrar Hashmi (Ph.D. Scholar in Electrical Engineering Department, CUST, Islamabad, Pakistan) and Usman Zafar (Ph.D. Scholar in Electrical Engineering Department, IST, Islamabad) for their valuable discussion throughout the research work.

REFERENCES

[1] S. Samadi, M. R. Khosravi, J. A. Alzubi, O. A. Alzubi, and V. G. Menon, "Optimum range of angle tracking radars: A theoretical computing," *Int. J. Electr. Comput. Eng. (IJECE)*, vol. 9, no. 3, p. 1765, Jun. 2019.

[2] S. G. Bhatti and A. I. Bhatti, "Adaptive measurement noise covariance matrix R for JPDAF based multitarget tracking," in *Proc. Int. Conf. Electr., Commun., Comput. Eng. (ICECCE)*, Jul. 2019, pp. 12–16.

[3] A. Denk, "Detection and jamming low probability of intercept (LPI) radars," M.S. thesis, Dept. Syst. Eng., Naval Postgraduate Sch., Monterey, CA, USA, 2006.

[4] G. Schrick and R. G. Wiley, "Interception of LPI radar signals," in *Proc. IEEE Int. Conf. Radar*, May 1990, pp. 108–111.

[5] D. E. Lawrence, "Low probability of intercept antenna array beamforming," *IEEE Trans. Antennas Propag.*, vol. 58, no. 9, pp. 2858–2865, Sep. 2010, doi: 10.1109/TAP.2010.2052573.

[6] D. C. Schleher, "LPI radar: Fact or fiction," *IEEE Aerosp. Electron. Syst. Mag.*, vol. 21, no. 5, pp. 3–6, May 2006.

[7] P. E. Pace, *Detecting and Classifying Low Probability of Intercept Radar*. Norwood, MA, USA: Artech House, 2009, pp. 123–135.

[8] G. Qiang, G. Xin, Z. Zheng-chao, and Z. Jing, "Study on emitter signal recognition based on rough sets and grey association theory," in *Proc. IEEE 10th Int. Conf. SIGNAL Process.*, Oct. 2010, pp. 2336–2340.

[9] F. Sagnard and J.-P. Tarel, "Template-matching based detection of hyperbolas in ground-penetrating radargrams for buried utilities," *J. Geophys. Eng.*, vol. 13, no. 4, pp. 491–504, Jul. 2016. Accessed: Jun. 10, 2021, doi: 10.1088/1742-2132/13/4/491.

[10] W. Wei and J. M. Mendel, "A fuzzy logic method for modulation classification in nonideal environments," *IEEE Trans. Fuzzy Syst.*, vol. 7, no. 3, pp. 333–344, Jun. 1999.

[11] L. Cohen, "Time-frequency distributions-a review," *Proc. IEEE*, vol. 77, no. 7, pp. 941–981, Jul. 1989.

[12] J.-D. Zhu, Y. Zhao, J. Tang, and J. Xu, "Automatic recognition of radar signals based on time-frequency image shape character," *Defence Sci. J.*, vol. 63, no. 3, pp. 308–314, May 2013.

[13] C. Wang, J. Wang, and X. Zhang, "Automatic radar waveform recognition based on time-frequency analysis and convolutional neural network," in *Proc. IEEE Int. Conf. Acoust., Speech Signal Process. (ICASSP)*, Mar. 2017, pp. 2437–2441.

[14] Z. Zhou, G. Huang, H. Chen, and J. Gao, "Automatic radar waveform recognition based on deep convolutional denoising auto-encoders," *Circuits, Syst., Signal Process.*, vol. 37, no. 9, pp. 4034–4048, Jan. 2018, doi: 10.1007/s00034-018-0757-0.
[15] G. López-Risueño, J. Grajal, and A. Sanz-Osorio, "Digital channelized receiver based on time-frequency analysis for signal interception," *IEEE Trans. Aerosp. Electron. Syst.*, vol. 41, no. 3, pp. 879–898, Jul. 2005.
[16] M. Zhang, L. Liu, and M. Diao, "LPI radar waveform recognition based on time-frequency distribution," *Sensors*, vol. 16, no. 10, p. 1682, Jul. 2016.
[17] R. G. Stockwell, "A basis for efficient representation of the S-transform," *Digit. Signal Process.*, vol. 17, no. 1, pp. 371–393, 2007.
[18] T. Oberlin, S. Meignen, and V. Perrier, "The Fourier-based synchrosqueezing transform," in *Proc. IEEE Int. Conf. Acoust., Speech Signal Process. (ICASSP)*, May 2014, pp. 40–44.
[19] M. Zhang, M. Diao, L. Gao, and L. Liu, "Neural networks for radar waveform recognition," *Symmetry*, vol. 9, no. 5, p. 75, May 2017.
[20] S.-H. Kong, M. Kim, L. M. Hoang, and E. Kim, "Automatic LPI radar waveform recognition using CNN," *IEEE Access*, vol. 6, pp. 4207–4219, 2018.
[21] J. Lunden and V. Koivunen, "Automatic radar waveform recognition," *IEEE J. Sel. Topics Signal Process.*, vol. 1, no. 1, pp. 124–136, Jun. 2007.
[22] X. Wang, G. Huang, Z. Zhou, W. Tian, J. Yao, and J. Gao, "Radar emitter recognition based on the energy cumulant of short time Fourier transform and reinforced deep belief network," *Sensors*, vol. 18, no. 9, p. 3103, Sep. 2018.
[23] T. Alrubeaan, K. Albagami, A. Ragheb, S. Aldosari, M. Altamimi, and S. Alshebeili, "An investigation of LPI radar waveforms classification in RoF channels," *IEEE Access*, vol. 7, pp. 124844–124853, 2019.
[24] S. Zhang, J. Pan, Z. Han, and L. Guo, "Recognition of noisy radar emitter signals using a one-dimensional deep residual shrinkage network," *Sensors*, vol. 21, no. 23, p. 7973, Nov. 2021.
[25] G. Kong and V. Koivunen, "Radar waveform recognition using Fourier-based synchrosqueezing transform and CNN," in *Proc. IEEE 8th Int. Workshop Comput. Adv. Multi-Sensor Adapt. Process. (CAMSAP)*, Dec. 2019, pp. 110–114.
[26] Z.-M. Liu and P. S. Yu, "Classification, denoising, and deinterleaving of pulse streams with recurrent neural networks," *IEEE Trans. Aerosp. Electron. Syst.*, vol. 55, no. 4, pp. 1624–1639, Aug. 2019.
[27] G. Ruan, Y. Wang, S. L. Wang, Y. Zheng, Q. Guo, and S. N. Shulga, "Automatic recognition of radar signal types based on CNN-LSTM," *Telecommun. Radio Eng.*, vol. 79, no. 4, pp. 305–321, 2020.
[28] Z. Ma, Z. Huang, A. Lin, and G. Huang, "LPI radar waveform recognition based on features from multiple images," *Sensors*, vol. 20, no. 2, p. 526, Jan. 2020.
[29] S. G. Bhatti and A. I. Bhatti, "BiLSTM based phase modulation detection of radar emitters," presented at the CIE Int. Conf. Radar, Haikou, China, Dec. 2021.
[30] N. Levanon and E. Mozeson, *Radar Signals*, 3rd ed. New York, NY, USA: Wiley, 2007, pp. 105–160.
[31] M. Hua, K. W. Yang, M. Wang, and K. J. Zou, "Analysis of the frequency offset effect on Zadoff–Chu sequence timing performance," 2014, *arXiv:1406.3412*.
[32] L. Liu, S. Wang, and Z. Zhao, "Radar waveform recognition based on time-frequency analysis and artificial bee colony-support vector machine," *Electronics*, vol. 7, no. 5, p. 59, Mar. 2018.
[33] L. Durak and O. Arikan, "Short-time Fourier transform: Two fundamental properties and an optimal implementation," *IEEE Trans. Signal Process.*, vol. 51, no. 5, pp. 1231–1242, May 2003.
[34] R. Tao, Y.-L. Li, and Y. Wang, "Short-time fractional Fourier transform and its applications," *IEEE Trans. Signal Process.*, vol. 58, no. 5, pp. 2568–2580, May 2010.
[35] S. Hochreiter and J. Schmidhuber, "Long short-term memory," *Neural Comput.*, vol. 9, no. 8, pp. 1735–1780, 1997.

SIDRA GHAYOUR BHATTI (Member, IEEE) received the B.S. degree in telecommunication engineering from the University of Engineering and Technology, Taxila, in 2013, and the M.S. degree in electrical engineering from the Capital University of Science and Technology (CUST), Islamabad, in 2019, where she is currently pursuing the Ph.D. degree. Since 2019, she has been a Research Assistant with the Control and Signal Processing Research Group, CUST. Her research interests include machine learning, radar signal processing, and communication.

AAMER IQBAL BHATTI (Senior Member, IEEE) received the M.S. degree in control systems from Imperial College London, London, U.K., in 1994, and the Ph.D. degree in control engineering from Leicester University, Leicester, U.K., in 1998.

Since 2007, he has been a Professor with the Department of Electrical Engineering, Capital University of Science and Technology, Islamabad, Pakistan. He is currently the pioneering Head of the Control and Signal Processing Research Group, CASPR Dynamics, Islamabad. His research interests include GSR development, radar signal processing, line echo canceller design, GSM audio codes, dynamic system modeling, and large diesel systems.